A Novel Triad Twisted String Actuator for Controlling a Two Degrees of Freedom Joint: Design and Experimental Validation*

Damian Crosby[1], Joaquin Carrasco[2], William Heath[2], and Andrew Weightman[2]

***Abstract*— Actuated universal joints, or equivalent joint systems, are found in a number of robotic applications, in particular mobile snake robots, snake-arm robots and robotic tails. These joints have two degrees of freedom on two axes, each perpendicular to a third axis and to themselves. Such joints use a variety of actuation methods, including direct drive motors, linear screw drives, cable based systems, and hydraulics/pneumatics. In this paper the authors design and validate a mechanism that uses the Twisted String Actuator (TSA) in an antagonistic triad to actuate the universal joint, using orientation sensors and load cells to create a robust cascading closed loop control system. This results in a light, compact, high-performance actuation system that avoids the extra mass and hardware complexity that alternative actuation methods present, with the additional challenge of non-linearity.**

I. Introduction

Actuated Universal Joint (AUJ) mechanisms are found in a wide range of robotic applications, such as confined space inspection using snake-arm robots [1], highly manoeuvrable mobile snake robots [2], and biomimetic robot tails for stability [3]. Mobile snake robots must usually incorporate electric actuators inline with their joints. This results in an AUJ having to shift the mass of the follower segments and all the actuators inside the follower segments, which results in high torque requirements and therefore Snake-arm robots and robotic tails can reduce the mass and size of the AUJ by moving their actuators away from the AUJs and use cables to transfer the force to the joints, or use hydraulic or pneumatic actuators which tend to be lighter than equivalent electric motors, at the expense of increased mass and bulk at the base of the arm or tail.

First developed by Würtz, May, Holz, *et al.* [4] in 2010, the Twisted String Actuator (TSA) uses two or more strings between two fixtures as a linear actuator. When one fixture is rotated (typically by an electric motor), the looped string twists into a helix, decreasing the distance between them.

The primary advantage of TSA over similar linear actuators such as a leadscrew is the reduction the TSA provides is not proportional (or even slightly inversely proportional) to the mass of the actuator. By decreasing r_s (or r_s+r_c when there are more than two strings, where r_c is the "core radius", or half the gap between any two strings that intersects the axis of rotation) the reduction increases for a constant l_u and θ_s, resulting in a greater reduction with no increase, or even a slight decrease, in actuator mass. While the reduction in a leadscrew can be increased by decreasing the lead on the thread (typically denoted as λ) which also has no increase in mass, this has a limited range and can quickly run up against manufacturing tolerances or material strength requirements. In order to achieve greater or more robust reductions, the screw radius has to be increased, or the driving motor has to have a larger reduction before driving the screw, both of which usually result in more material (typically steel) and therefore more mass.

However, TSA does have some disadvantages, the most significant of which is a non-linear reduction equation, which is also dependent on the motor angle θ_s (and therefore actuator position). The reduction decreases in a non-linear fashion as the angle increases, with the derivative decreasing as the angle increases. There is also the compliance of the strings to consider, depending on the thickness and material chosen, which becomes a significant factor under high forces. Both of these issues can be addressed with accurate modelling [5] and/or a robust control strategy, as demonstrated in [4]. What is perhaps more an issue regarding mass for an AUJ is the unidirectional force of the TSA, which can only impart force in tension. This means that for an AUJ, which is a two degree of freedom joint, a minimum of three TSA are required for unless spring return mechanisms are used, which would impart additional force on the TSA and therefore reduce performance. However, the potential high force to mass ratio of the TSA due to the non-proportional reduction may adequately compensate for the additional actuator requirement.

The focus of this research is to investigate if the TSA is a suitable candidate for control of an AUJ considering both the benefits and drawbacks.

To this end, the objective is to simulate a model and then construct a physical experimental prototype to validate the proposed control system.

A. Twisted String Actuator

First developed by [4] in 2010, TSA uses two or more strings between two fixtures as a linear actuator. When one fixture is rotated (typically by an electric motor), the

*This work was supported by the UKRI EPSRC DTP, award reference 1957210.

[1]Department of Mechanical, Aerospace and Civil Engineering, University of Manchester, United Kingdom.

[2]Department of Electrical and Electronic Engineering, University of Manchester, United Kingdom.

Email correspondence: damian.crosby@manchester.ac.uk

strings twist into a helix, decreasing the distance between the fixtures.

The following equation from [4] calculates the actuator length l_s for a given θ_s, given l_u and r_s for a two string TSA. This equation assumes an infinite string stiffness, so is only reasonably accurate under low tension.

$$l_s(\theta_s) = \sqrt{l_u^2 - \theta_s^2 r_s^2} \tag{1}$$

Although theoretically the stroke of the TSA can be the entire domain of $[0, l_u]$, in reality the thickness of the string prevents a geometric helix from forming once the helix pitch $q < 4r_s$ (or $q < 2nr_s$ for n strings). This limits the lower bound of the stroke to the value in the following equation, or approximately 46% of l_u for a two string TSA.

$$l_{min} = \frac{l_u}{\sqrt{\frac{\pi^2}{2} + 1}} \approx 0.46\ l_u \tag{2}$$

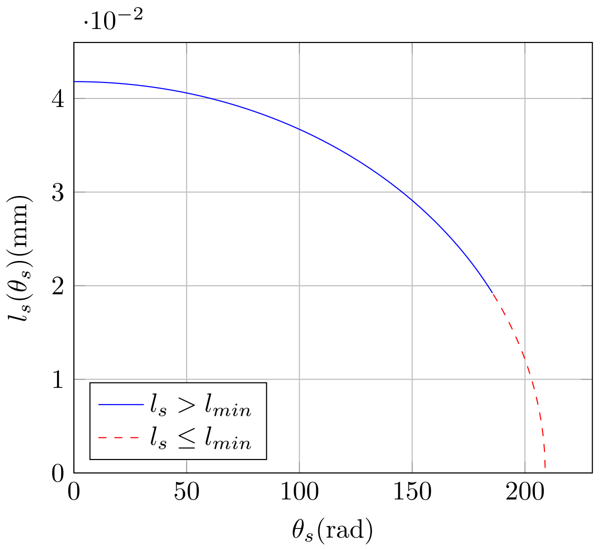

Fig. 1: TSA string length against motor angle with coefficients from table I.

B. Antagonstic Triad

As mentioned in the introduction, because the TSA provides only tensile force, a minimum of three actuators are required. These can be arranged in a triangular configuration to create an "antagonistic triad", akin to the antagonistic pairs of muscles found in animals. Where a revolute joint would be found between the connecting ends of the actuator, a universal joint is found instead. The geometric structure of the system can be described with two equilateral triangles of inradius r on two planes separated in the z axis. The centroids are then connected via a universal joint from each plane normal to an intersecting point, described by vector $\boldsymbol{\theta} = \begin{bmatrix}\theta_1 & \theta_2\end{bmatrix}$ to denote the rotation of the second plane relative to the first, in the x and y axis around the intersecting point, and l_1 and l_2 to denote the normal distance from the intersection to the first and second plane centroids respectively. When $\boldsymbol{\theta} = \begin{bmatrix}0 & 0\end{bmatrix}$ the triangles are parallel to each other. The distance between the vertex pairs of each triangle is then denoted as $\begin{bmatrix}\lambda_1 & \lambda_2 & \lambda_3\end{bmatrix}$ for the "top", "left" and "right" vertices of the triangles. When $\boldsymbol{\theta}$ is changed, this will change λ_1, λ_2 and λ_3 respectively. Figure 2 illustrates this antagonistic triad.

To calculate the lengths of the strings for a given $\boldsymbol{\theta}$ of the universal joint, we can define a vector function $\Lambda(\boldsymbol{\theta}) = \begin{bmatrix}\lambda_1(\boldsymbol{\theta}) & \lambda_2(\boldsymbol{\theta}) & \lambda_3(\boldsymbol{\theta})\end{bmatrix}$ with l_1, l_2 and r as the coefficients.

$$\begin{aligned}
\lambda_1(\boldsymbol{\theta}) &= \sqrt{\begin{aligned}&(l_1 + l_2\cos\theta_1\cos\theta_2 + r\cos\theta_1\sin\theta_2)^2\\ &+ (r - r\cos\theta_2 + l_2\sin\theta_2)^2\\ &+ (l_2\cos\theta_2\sin\theta_1 + r\sin\theta_1\sin\theta_2)^2\end{aligned}}\\
\lambda_2(\boldsymbol{\theta}) &= \sqrt{(a-b+c)^2 + (l_1-d)^2 + (e)^2}\\
\lambda_3(\boldsymbol{\theta}) &= \sqrt{(a+b-c)^2 + (l_1+d)^2 + (e)^2}\\
&\text{where:}\\
&\quad a = -\tfrac{\sqrt{3}r(\cos\theta_1 - 1)}{2}\\
&\quad b = l_2\cos\theta_2\sin\theta_1\\
&\quad c = \tfrac{r\sin\theta_1\sin\theta_2}{2}\\
&\quad d = \tfrac{\sqrt{3}r\sin\theta_1}{2} + l_2\cos\theta_1\cos\theta_2 - \tfrac{r\cos\theta_1\sin\theta_2}{2}\\
&\quad e = \tfrac{r\cos\theta_2}{2} - \tfrac{r}{2} + l_2\sin\theta_2
\end{aligned} \tag{3}$$

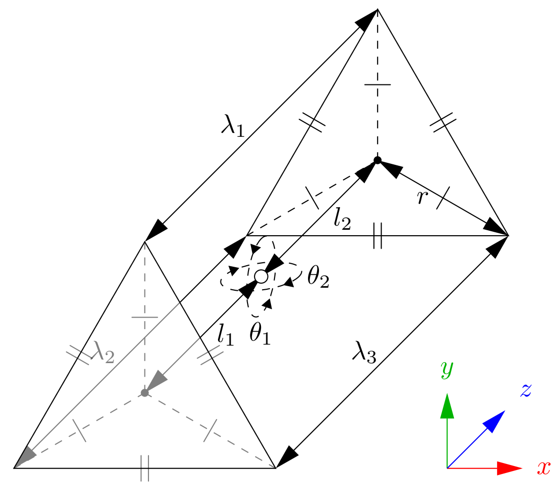

Fig. 2: Kinematic diagram of the antagonistic triad, where the universal joint rotation is defined by $\theta_{1,2}$ on the x and y axes respectively, and the string lengths are defined by $\lambda_{1,2,3}$ for the "Top", "Left" and "Right" strings. r and $l_{1,2}$ define the anchor points of the strings.

II. Control System

The control system is a four layer cascade design, using feedback of the joint position from the accelerometers and TSA force from the load cells. It uses a second

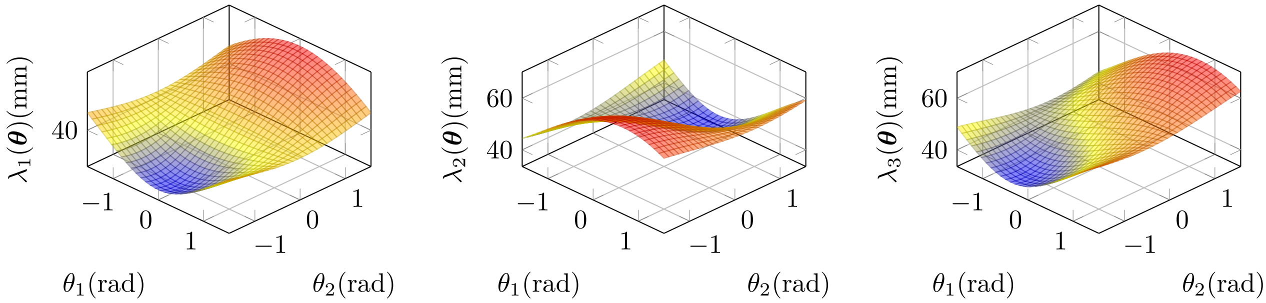

Fig. 3: Surface plots of each element of the vector function $\Lambda(\boldsymbol{\theta})$, assuming coefficient values from table I.

order setpoint trajectory $\boldsymbol{q}$ as input, which can either be pre-defined or generated dynamically from user input. Feedback is provided by the AUJ angular position $\boldsymbol{\theta}$, angular velocity $\dot{\boldsymbol{\theta}}$, and TSA tension force $\hat{\boldsymbol{f}}$.

A. Actuated Universal Joint Position PID Controller with Acceleration Feedforward

Firstly, a PID controller is used to generate a control signal $\boldsymbol{u}$ with the input $\boldsymbol{q}$ as the setpoint, and the AUJ angular position $\boldsymbol{\theta}$ and velocity $\dot{\boldsymbol{\theta}}$ as feedback, plus the addition of a feedforward term for the input acceleration $\ddot{\boldsymbol{q}}$.

$$\boldsymbol{u} = \boldsymbol{k}_p\left(\boldsymbol{q} - \boldsymbol{\theta}\right) + \boldsymbol{k}_i\left(\int_0^t \boldsymbol{q} - \boldsymbol{\theta}\right)dt + \boldsymbol{k}_d\left(\dot{\boldsymbol{q}} - \dot{\boldsymbol{\theta}}\right) + \ddot{\boldsymbol{q}} \quad (4)$$

B. Inverse Dynamics

The control signal $\boldsymbol{u}$ from the PID controller is then converted to the desired AUJ torque $\boldsymbol{\tau}$ using the Euler-Lagrange method.

$$\boldsymbol{\tau} = D\left(\boldsymbol{\theta}\right)\boldsymbol{u} + C\left(\boldsymbol{\theta}, \dot{\boldsymbol{\theta}}\right)\dot{\boldsymbol{\theta}} + G\left(\boldsymbol{\theta}\right) \quad (5)$$

C. Twisted String Actuator Force Optimisation Algorithm

This function uses a modified algorithm from [6] to select an optimal force vector from the desired joint torque. A force matrix F is created from the torque input $\boldsymbol{\tau}$, jacobian J_Λ from the vector function Λ as defined in equation 3, and minimum force constant f_{min}. f_{ii} is equal to f_{min}, while the other elements in the column are based on a calculation using $J_{\Lambda_{-i,*}}$ where $-i$ is a row removed from the matrix.

$$\begin{aligned}
J_\Lambda &= \begin{bmatrix} \frac{\partial\lambda_1}{\partial\theta_1} & \frac{\partial\lambda_2}{\partial\theta_1} & \frac{\partial\lambda_3}{\partial\theta_1} \\ \frac{\partial\lambda_1}{\partial\theta_2} & \frac{\partial\lambda_2}{\partial\theta_2} & \frac{\partial\lambda_3}{\partial\theta_2} \end{bmatrix} \\
\boldsymbol{F}\left(\boldsymbol{\tau}, \boldsymbol{\theta}\right) &= \begin{cases} f_{i,i} = f_{min} \\ f_{-i,i} = -J_{\Lambda_{-i,*}}^{-\intercal}\left(J_{\Lambda_{i,*}}^{\intercal} f_{min} + \boldsymbol{\tau}\right) \end{cases} \\
&= \begin{bmatrix} f_{min} & f_{12} & f_{13} \\ f_{21} & f_{min} & f_{23} \\ f_{31} & f_{32} & f_{min} \end{bmatrix}
\end{aligned} \quad (6)$$

The following algorithm then selects one column of $\boldsymbol{F}$ to be the output force vector $\boldsymbol{f}$.

$\boldsymbol{s} \leftarrow \begin{bmatrix} \top & \top & \top \end{bmatrix}$
if $f_{23} > f_{min}$ **then** $s_2 \leftarrow \bot$ **else** $s_3 \leftarrow \bot$ **end if**
if $f_{31} > f_{min}$ **then** $s_3 \leftarrow \bot$ **else** $s_1 \leftarrow \bot$ **end if**
if $f_{12} \geq f_{min}$ **then** $s_1 \leftarrow \bot$ **else** $s_2 \leftarrow \bot$ **end if**
for $i = 1$ to 3 **do**
    if $s_i \rightarrow \top$ **then** $\boldsymbol{f} \leftarrow \boldsymbol{f}_{*,i}$ **end if**
end for

D. Twisted String Actuator Force Proportional Controller

The selected forces are then used as an input to a P controller using the measured load cell forces $\hat{\boldsymbol{f}}$ as feedback. The output from this can then be used to control the top, left and right TSA motors.

1) Simulation Current Control: In the simulation, each TSA was modelled as a state-space system which takes motor current u as an input and outputs y as the TSA tension force. [4] defines it as such, where J is the motor inertia, C is the motor coulomb friction (modified from viscous friction as the 1724TSR only has dry friction), K_t is the motor torque constant, and K_L is the load stiffness. As the original definition is for a fixed load l_u distance from the motor a modified model is required which takes into account the varying length between the motor and load defined by $\Lambda(\boldsymbol{\theta})$. A saturation function is used to prevent incorrect compression forces when the string is slack. All of the motor coefficients were taken from the Faulhaber 1724TSR datasheet [7] as this is the motor used in the experimental model. An estimated value is used for the load stiffness, this was chosen to be a high number as the model is expected to be very stiff.

$$\begin{aligned}
h\left(\theta_s\right) &= \frac{\theta r_s^2}{\sqrt{l_u^2 - \theta_s^2 r_s^2}} \\
k\left(\theta_s, \boldsymbol{\theta}\right) &= \lambda_n\left(\boldsymbol{\theta}\right) - \sqrt{l_u^2 - \theta_s^2 r_s^2} \\
\dot{\boldsymbol{x}} &= \begin{bmatrix} x_2 \\ -\frac{K_L}{J} h\left(x_1\right) k\left(x_1, \boldsymbol{\theta}\right) - \frac{C}{J}\operatorname{sgn}\left(x_2\right) \end{bmatrix} + \begin{bmatrix} 0 \\ \frac{K_t}{J} \end{bmatrix} u \\
y &= K_L \operatorname{sat}_0^\infty k\left(x_1, \boldsymbol{\theta}\right)
\end{aligned} \quad (7)$$

TABLE I: Model coefficients.

Coefficient	Value	Coefficient	Value
l_1	41.8 mm	J	1×10^{-6} kg m^{-2}
l_2	0 mm	K_L	1000 N m^{-1}
r	13 mm	f_{min}	3 N
l_u	41.8 mm	ω_s	441.9 rad s^{-1}
r_s	200 µm	I_s	0.19 A
m	72.619 13 g	K_t	0.0263 N m A^{-1}
C	0.1315 N mm	τ_s	4.5 mN m
α_s	1×10^5 rad s^{-2}		
Coefficient	**Value**		
I	$\begin{bmatrix} 3\times10^{-5} & 0 & 0 \\ 0 & 3.2\times10^{-5} & 0 \\ 0 & 0 & 1.4\times10^{-5} \end{bmatrix}$ kg m^{-2}		

TABLE II: PID gains in the simulation and experiment.

Gain	Value	
	Simulation	Experiment*
k_p	800	3×10^4
k_i	3000	350
k_d	50	50
k_{p_s}	19	100

* Tracking mode, see section III-B.

The state space model was then adapted to include constraints on motor velocity and acceleration set by the motor controller in order to keep the motor within design limits, by replacing $\dot{\boldsymbol{x}}$ with $\dot{\boldsymbol{x}}'$ which contains saturation functions for maximum motor velocity v_s and acceleration α_s.

$$\dot{\boldsymbol{x}}' = \begin{bmatrix} \mathrm{sat}_{\omega_s}\, \dot{x}_1 \\ \mathrm{sat}_{\alpha_s}\, \dot{x}_2 \end{bmatrix} \tag{8}$$

2) Experimental Velocity Control with Deadband Compensation: In the experimental model, current control did not result in a stable output, so instead the P controller output would be the motor velocity as $\boldsymbol{\omega}$ (each motor controller has a hardware velocity PI controller). Due to a hardware velocity controller deadband within $\pm 10\,\mathrm{min}^{-1}$, an adjustable deadband compensator is used to create $\bar{\boldsymbol{\omega}}$, with $h \in [0, 10]$ changing the size of the deadband, where 0 is no deadband, and 10 is full deadband.

$$\bar{\boldsymbol{\omega}} = \boldsymbol{\omega} \mid \omega_i \begin{cases} \omega_i & \omega_i > 10 \vee \omega_i < -10 \\ 10 & \omega_i < 10 \wedge \omega_i > h \\ -10 & \omega_i > -10 \vee \omega_i < -h \\ 0 & \text{otherwise} \end{cases} \tag{9}$$

The result from the TSA is then a compressive force acting between each of the three TSA and its corresponding endpoint on the Antagonistic Triad, imparting a torque on the axes of the universal joint.

TABLE III: PID constants for both states.

Gain	Value	
	Windup	Tracking
k_p	800	3×10^4
k_i	3000	350

III. Simulation & Experimental Results

A. Experimental Setup

For the experimental validation, a physical prototype of the mechanism was constructed with coefficients from table I as design parameters. This was mounted vertically, in order for the Inertial Measurement Unit (IMU) to measure the orientation of the universal joint. The TSA mechanisms consist of a high torque motor attached to the base segment, with a string clamp attached to the motor shaft. On the follower segment, a load cell is mounted on top of a universal joint to ensure a purely axial load, with a capstan bolt attached to the load cell. The string itself is attached to the clamp at both ends using two grub screws for extra security and easy adjustment, and looped through the hole in the capstan bolt.

B. Windup & Tracking States

When the mechanism is started with the TSA in a completely unwound state, before it can begin tracking a motion trajectory, the TSA strings must "wind up" to closely match the intial state of $\boldsymbol{f}$. During this phase, the outer PID gains $\boldsymbol{k}_p, \boldsymbol{k}_i$ are unsuitable and can result in damage to the mechanism. To mitigate this, two sets of PID gains are chosen, one for the windup state, and another for the tracking state, which the windup state transitions to once suitable stability is achieved. This transition trigger is defined on a per-axis basis, as the first zero crossing of the angle error (as $\boldsymbol{q} = 0$ this is effectively $\boldsymbol{\theta}$).

C. Results

Figure **??** plots the tracking response of both the simulation and experiment. Three trajectories were created to test the capabilites of the mechanism. Two were only in one axis of the Universal Joint, and the third was in both axes. The deflection angle range was limited due to the low value of l_u, but can easily be extended by increasing this value. A low l_u was chosen as it resulted in easier installation.

IV. Experimental Testing and System Validation

A. Performance Comparison

The two most important performance metrics are the maximum tension force f_{max} and maximum stroke velocity $\dot{p}_{max}$. For both the TSA and leadscrew $f_{max} \propto \frac{1}{\dot{p}_{max}}$ holds true as the mutable coefficients are changed for the AUJ, so finding a balance between these two metrics is

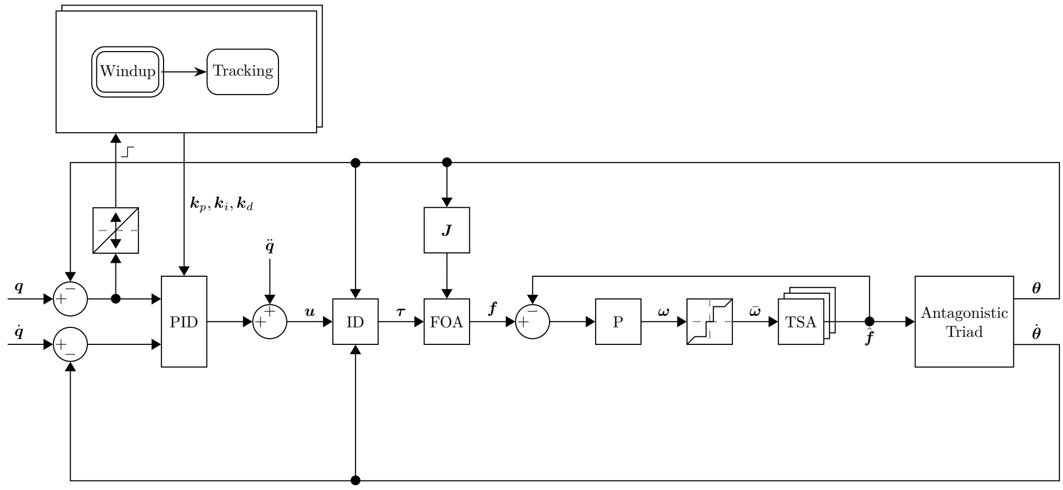

Fig. 4: Block diagram of the complete experimental control system, excluding the hardware velocity controllers for the motors.

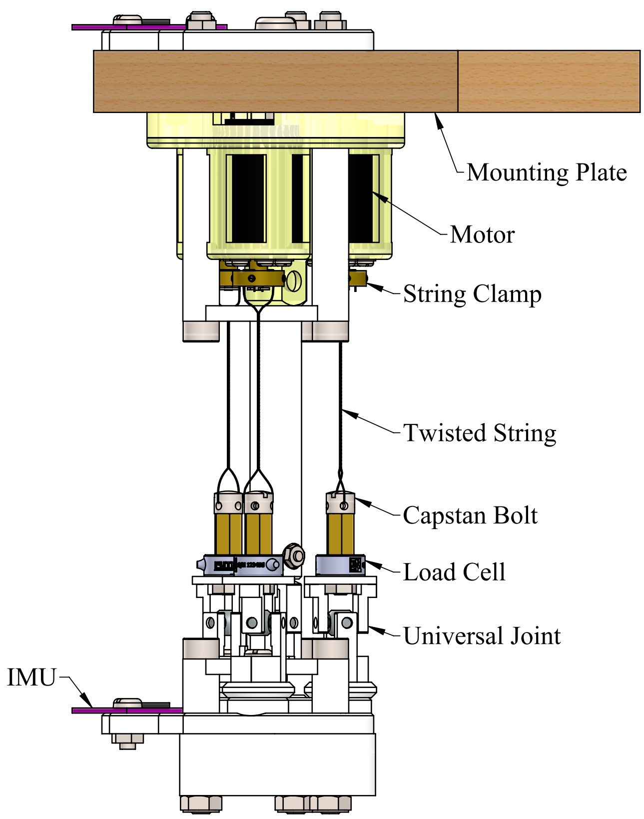

Fig. 5: Schematic of the experimental model with labelled components.

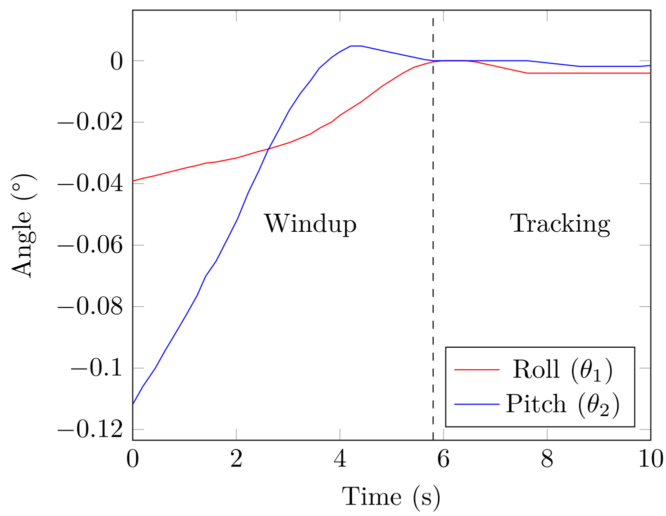

Fig. 6: The inital startup of the mechanism showing the transition between “windup” and “tracking” states.

required. These are dependant on the maximum motor torque τ_{max} and motor velocity $\dot{\theta}_{max}$.

For the TSA metrics, the equations from [4], in particular $h(\theta)$ and $k(\theta)$ as used for the State Space in equation **??**, which can be used to determine f_{max} and $\dot{p}_{max}$ using equations **??** and **??**. By extracting coefficient r_s as an input to make $f(p, r_s)$ and $\dot{p}(\dot{\theta}, p, r_s)$ the performance of different string thicknesses can be compared for a given unwound length l_u and $\tau_{max}, \dot{\theta}_{max}$ over the range of the contraction length p.

For the leadscrew metrics, the raising torque calculation can be used as the absolute value of f_{max}, since the TSA only operates in tension, which can be used to determine the same metrics using equation **??**. The performance of different screw diameters d_m and leads λ can then be compared for a given τ_{max}. $\dot{p}_{max}$ is then calculated by multiplying λ with $\dot{\theta}_{max}$. The performance of different λ can then be compared for a given $\dot{\theta}_{max}$.

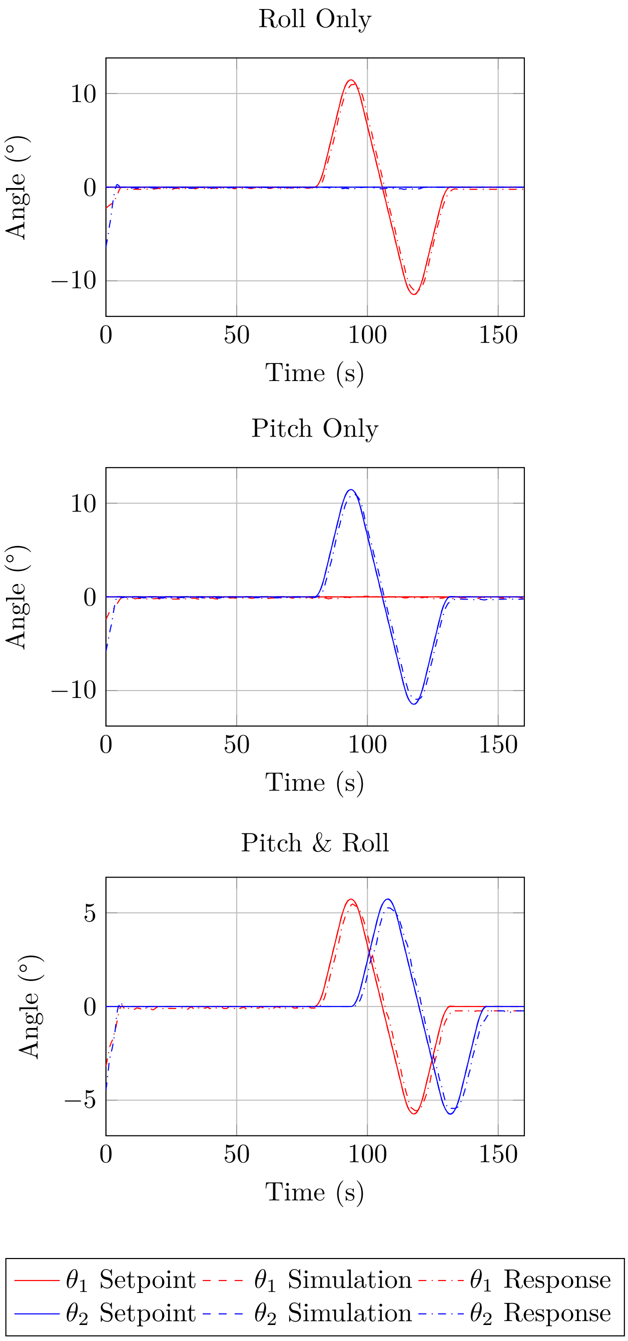

Fig. 7: Plots of the response for three different trajectories, one on only the roll axis, one on only the pitch axis, and one on both axes.

$$\begin{aligned}
k(\theta) &= l_u - \sqrt{l_u^2 - \theta_s^2 r_s^2} \\
k^{-1}(p) &= \pm \frac{\sqrt{p(2l_u - p)}}{r_s} \\
h^{-1}(\theta) &= \frac{\sqrt{l_n^2 - r_s^2\theta^2}}{r_s^2\theta} \\
f(p) &= h^{-1}\left(k^{-1}(p)\right) = \pm \frac{\sqrt{(l_u - p)^2}}{r_s\sqrt{p(2l_u - p)}} \\
f_{max} &= f(p)\tau_{max}
\end{aligned} \tag{10}$$

$$\begin{aligned}
\dot{k}\left(\dot{\theta}, \theta\right) &= \frac{\dot{\theta} r_s^2 \theta}{\sqrt{l_n^2 - r_s^2\theta^2}} \\
\dot{p}\left(\dot{\theta}, p\right) &= \dot{k}\left(\dot{\theta}, k^{-1}(p)\right) = \pm \frac{\dot{\theta} r_s \sqrt{p(2l_n - p)}}{\sqrt{(l_n - p)^2}} \\
\dot{p}_{max} &= \dot{p}\left(\dot{\theta}_{max}, p\right)
\end{aligned} \tag{11}$$

$$\begin{aligned}
|\tau(f)| &= \frac{d_m f(\lambda + \pi d_m \mu)}{2(\pi d_m - \lambda\mu)} \\
|f(\tau)| &= \frac{2\tau(\pi d_m - \lambda\mu)}{d_m(\lambda + \pi d_m \mu)} \\
f_{max} &= |f(\tau_{max})|
\end{aligned} \tag{12}$$

$$\begin{aligned}
\dot{p}\left(\dot{\theta}\right) &= \lambda \frac{\dot{\theta}}{2\pi} \\
\dot{p}_{max} &= \dot{p}\left(\dot{\theta}_{max}\right)
\end{aligned} \tag{13}$$

As the values for τ_{max} and $\dot{\theta}_{max}$ for the TSA depend on p, but remain constant for the leadscrew, the performance of the TSA is going to be better or worse than a given leadscrew depending on the value p. Figure **??** compares the TSA configuration using the coefficients from table **??** against a number of common leadscrew configurations that are practical for the dimensions of the AUJ. As can be noted, the TSA outperforms or underperforms different leadscrew configurations depending on p.

V. Conclusion

References

[1] R. O. Buckingham and A. C. Graham, “Dexterous manipulators for nuclear inspection and maintenance — case study,” in *2010 1st International Conference on Applied Robotics for the Power Industry*, 2010, pp. 1–6.

[2] M. Luo, R. Yan, Z. Wan, *et al.*, “Orisnake: Design, fabrication, and experimental analysis of a 3-d origami snake robot,” *IEEE Robotics and Automation Letters*, vol. 3, no. 3, pp. 1993–1999, 2018.

[3] W. S. Rone, W. Saab, and P. Ben-Tzvi, “Design, Modeling, and Integration of a Flexible Universal Spatial Robotic Tail,” *Journal of Mechanisms and Robotics*, vol. 10, no. 4, Apr. 2018, 041001, ISSN: 1942-4302. DOI: `10.1115/1.4039500`. eprint: `https://asmedigitalcollection.asme.org/mechanismsrobotics/article-pdf/10/4/041001/6259163/jmr\_010\_04\_041001.pdf`. [Online]. Available: `https://doi.org/10.1115/1.4039500`.

[4] T. Würtz, C. May, B. Holz, C. Natale, G. Palli, and C. Melchiorri, “The twisted string actuation system: Modeling and control,” in *2010 IEEE/ASME International Conference on Advanced Intelligent Mechatronics*, 2010, pp. 1215–1220. DOI: `10.1109/AIM.2010.5695720`.

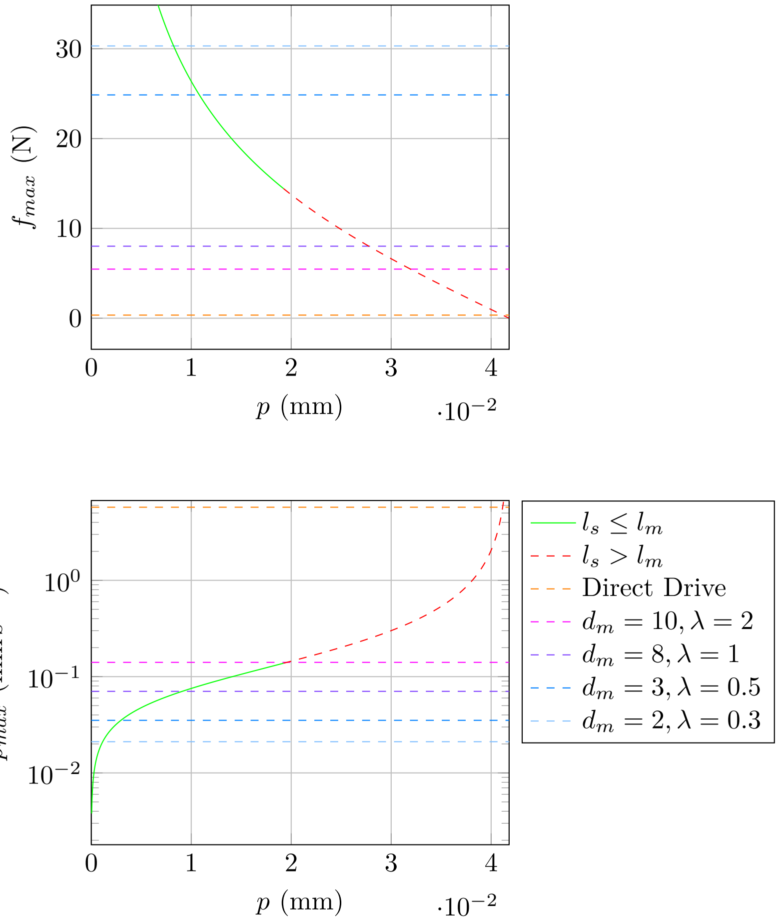

Fig. 8: Performance comparison of the TSA configuration using coefficients from table **??** to various leadscrew configurations with different d_m and λ.

[5] S. Nedelchev, I. Gaponov, and J. Ryu, "Accurate dynamic modeling of twisted string actuators accounting for string compliance and friction," *IEEE Robotics and Automation Letters*, vol. 5, no. 2, pp. 3438–3443, 2020. DOI: 10.1109/LRA.2020.2970651.

[6] F. Dessen, "Coordinating control of a two degrees of freedom universal joint structure driven by three servos," in *Proceedings. 1986 IEEE International Conference on Robotics and Automation*, vol. 3, 1986, pp. 817–822. DOI: 10.1109/ROBOT.1986.1087559.

[7] *Dc micromotors - precious metal commutation*, Dr. Fritz Fauhaber GmbH & Co. KG, Feb. 2020. [Online]. Available: https://www.faulhaber.com/fileadmin/Import/Media/EN_1724_SR_DFF.pdf.